



LAWRENCE
LIVERMORE
NATIONAL
LABORATORY

Modification of divertor heat and particle flux profiles with applied 3-D fields in NSTX H-mode plasmas

J.-W. Ahn, J. Canik, V. A. Soukhanovskii, R. Maingi, D. Battaglia

October 23, 2009

Nuclear Fusion

Disclaimer

This document was prepared as an account of work sponsored by an agency of the United States government. Neither the United States government nor Lawrence Livermore National Security, LLC, nor any of their employees makes any warranty, expressed or implied, or assumes any legal liability or responsibility for the accuracy, completeness, or usefulness of any information, apparatus, product, or process disclosed, or represents that its use would not infringe privately owned rights. Reference herein to any specific commercial product, process, or service by trade name, trademark, manufacturer, or otherwise does not necessarily constitute or imply its endorsement, recommendation, or favoring by the United States government or Lawrence Livermore National Security, LLC. The views and opinions of authors expressed herein do not necessarily state or reflect those of the United States government or Lawrence Livermore National Security, LLC, and shall not be used for advertising or product endorsement purposes.

Modification of divertor heat and particle flux profiles with applied 3-D fields in NSTX H-mode plasmas

J.-W. Ahn^{1*}, J. M. Canik¹, V. A. Soukhanovskii², R. Maingi¹, and D. J. Battaglia¹

¹Oak Ridge National Laboratory, Bethel Valley Road, Oak Ridge, TN 37831, USA

²Lawrence Livermore National Laboratory, 7000 East Ave., Livermore, CA 94551, USA

Abstract

Externally imposed non-axisymmetric magnetic perturbations are observed to alter divertor heat and particle flux profiles in the National Spherical Torus Experiment. The applied 3-D field induced multiple peaks in divertor profiles, characteristic of strike point splitting and “magnetic lobe” structure. The measured heat flux profile shows that the radial location and spacing of the striations are qualitatively consistent with a vacuum field tracing calculation. 3-D field application modestly reduced the peak divertor heat and particle fluxes. Spatial characteristics of the observed patterns are reported.

1. Introduction

The application of small, 3-D magnetic field perturbations produced by internal or external coils has been found to have significant impact on the plasma performance in tokamaks. As the present plan for the International Thermonuclear Experimental Reactor (ITER) relies on the use of non-axisymmetric magnetic perturbation for ELM suppression [1], the effect of these 3-D fields on the divertor heat and particle footprints on the divertor plates is of substantial interest.

In DIII-D [2], large type-I edge localized modes (ELMs) have been successfully eliminated [3,4,5,6] by applying resonant magnetic perturbations (RMPs) produced by a series of coils inside the vacuum vessel (internal or “I-coils”). In the National Spherical Torus Experiment (NSTX) [7], long ELM-free H-mode plasmas were achieved by heavy lithium evaporation and coating onto the plasma facing components [8]. Application of 3-D fields to these plasmas triggered ELMs [9,10,11] with the ELM frequency controlled by the frequency of applied 3-D field coil currents. ELMs are usually regarded as a threat to the plasma facing components because of their large transient heat flux. However, a continuous impurity build up in the core plasma during the ELM-free phase prevents sustained operation in high confinement

*Corresponding author’s contact information: jahn@pppl.gov, Princeton Plasma Physics Laboratory, MS-15, Princeton, NJ 08543, USA

mode or “H-mode” (in the absence of other cross field transport enhancements). This could be especially important in spherical tori, where it has been predicted that, due to the strong shaping and low aspect ratio, extremely high pedestal pressures may be achieved before ELM stability limits are reached [12]. Fortunately, ELM pace-making with 3-D field perturbations has been successfully demonstrated in NSTX as an impurity accumulation control tool [9,10,11].

When the external 3-D field is applied, its interaction with the pre-existing magnetic equilibrium produces a 3-D structure of perturbed magnetic field lines in the plasma edge, where the poloidal magnetic flux is re-organized into topological structures known as homoclinic tangles [13]. Perturbed by non-axisymmetric 3-D fields, the separatrix is split into multiple invariant manifolds forming a 3-D “lobe” structure for the open field lines, which are a mixture of long connection length stochastic field lines and short connection length laminar field lines. The lobe structure of the open field lines generates a striated strike point pattern radially across the divertor target surface. This structure is expected to be reflected in the measured divertor heat and particle flux profiles, due to the rapid parallel transport along the open field lines. Indeed, such an observation during the RMP application was recently reported [14] in DIII-D H-mode discharges. This result shows formation of striated strike point pattern for heat flux for high (>0.5) pedestal electron collisionality, $\nu_e^* = q_{95} R \epsilon^{-3/2} \lambda_{ee}^{-1}$, while particle flux showed striation for both high and low collisionalities. Here, R is the major radius, ϵ is the inverse aspect ratio ($\epsilon=a/R$), λ_{ee} is the electron mean free path.

In principle, 3-D fields can also be used to broaden both the heat and particle flux profiles. The remainder of this paper presents evidence affirming that statement. A high speed infrared (IR) camera was newly implemented [15] on NSTX, enabling measurement of the heat flux profiles during the application of a 3-D magnetic field. A 1-D CCD array also views the divertor plates to obtain D_α profiles [19]. This paper also reports the signatures of the magnetic lobe structure in the heat flux and D_α profiles in NSTX H-mode plasmas, as well as the effect of coil current variation on the observed lobe characteristics. In general the measured heat flux profile has characteristics expected from the lobe structure and strike point splitting, similar to the DIII-D result at high collisionality [14].

2. Experimental set-up

The effect of 3-D perturbative magnetic field was investigated in the low aspect ratio NSTX ($R=0.85\text{m}$, $a<0.67\text{m}$, $R/a>1.27$), where H-mode plasmas are routinely accessed [16] via good wall conditions, auxiliary heating power, flexible plasma position and shape controls. In these experiments, the toroidal magnetic field (B_t) at the magnetic axis was fixed at $\sim 0.4\text{T}$, and the

neutral beam injected power (P_{NBI}) of 4MW was used. Plasmas were highly shaped (elongation factor $\kappa \sim 2.4$, triangularity $\delta \sim 0.8$), and the plasma current was fixed at $I_p = 800\text{kA}$. The 3-D perturbation fields were generated with a set of six midplane coils, external but close-fitting to the vacuum vessel, that are typically used for error field correction and resistive wall mode feedback control [17,18]. The coils were configured to apply an $n=3$ field in the ELM-destabilization experiments, with a generated magnetic perturbation at the separatrix, $\delta B/B = 0.6-0.7\%$ for the peak δB at the coil center and in the order of 0.1% for the integrated δB over the coil surface. The poloidal spectrum of the applied magnetic perturbation is broad at the plasma edge, reaching high enough mode numbers to be resonant with high edge safety factor values ($q_{95} \sim 10$).

Figure 1 shows the poloidal cross section of NSTX showing the location of the diagnostic views as well as the external 3-D field coil. The magnetic equilibrium for a typical discharge is also overlaid. Also shown in figure 1 is the contour plot of the calculated connection lengths at the divertor surface using a vacuum field line following code with the application of external $n=3$ fields. The formation of 3-D lobe structure is clearly seen. The spatial coverage of the NSTX D_α (1-D) and IR (2-D) cameras is also overlaid.

The heat flux measurement is made with an SBF-161 IR camera [15], installed at toroidal angle $\varphi = 225^\circ$. The camera takes IR images of the lower divertor plates in 2-D with a temporal resolution of 1.6 to 6.3kHz (depending on the frame size). The front lens focal length of 25mm gives a 45° of circular field-of-view (FOV), with ~ 6.7 mm spatial resolution at the divertor target. The camera measures surface IR emission, which is converted to surface temperature from bench and in-situ calibrations. A 1-D heat conduction model is used to calculate the divertor heat flux profile from the surface temperature. The several kHz framing rate is a substantial improvement over the existing 30Hz frame IR cameras [19], and the improved temporal resolution enables heat flux measurement of transient events, such as ELMs and disruptions. The fast framing rate also facilitates measurement of the formation of the magnetic lobe structure in the heat flux profile, which starts to appear within 4-5ms after the 3-D field coil application.

The D_α emission at the lower divertor target is recorded by a 1-D CCD camera installed at $\varphi = 105^\circ$. It is operated at 2kHz rate and with sub-mm spatial resolution and is a part of the system of CCD arrays that are spectrally filtered for deuterium Balmer- α (656.1nm), Balmer- γ (433.9nm), and/or HeII Paschen- α (468.5nm) emission lines using $\Delta\lambda = 1.0-1.5\text{nm}$ bandpass interference filters [20]. The D_α emission is closely correlated with the particle flux in attached plasmas, due to its strong dependence on the plasma density.

3. Influence of non-axisymmetric field on heat flux and D_α profiles

The amplitude of the 3-D field perturbations was scanned by varying coil currents from 0.5kA to 1.0kA. Lithium wall conditioning/coating was used, provided by two lithium evaporators (LITERS) [21], to produce baseline ELM-free H-mode plasmas. The applied 3-D field was used to induce ELMs, and the effect of coil current amplitude and its application frequency on the ELM characteristics and the magnetic lobe structure were measured. The temporal evolution of a typical discharge is shown in Figure 2. The L-H transition is indicated by the drop of divertor D_α emission at ~ 110 ms, and the H-mode was sustained until ~ 570 ms. The 3-D field perturbation was applied at 400ms with constant amplitude of 0.75 kA. The D_α trace shows that periodic Type-I ELMs were triggered after 40-50ms following the application of 3-D fields. The line-average electron density continued to rise in the H-mode phase, despite the presence of triggered ELMs. Figure 3 shows profiles of the electron temperature (T_e), density (n_e), ion temperature (T_i), and electron collisionality (ν_e^*), immediately before and after the application of n=3 field. Before applying n=3 perturbative fields, the electron collisionality near the density pedestal top ($R\sim 1.45$ m) is 0.2-0.3. ν_e^* in the steep gradient region ($R\sim 1.46$ m) is around 1. It is observed that the edge electron collisionality dropped after the application of 3-D field while the core is not affected and the change in the whole T_i profile is also not seen.

Figure 4 compares the lower divertor IR emission before and after the application of 3-D field perturbation. Striation in the IR image following the perturbation is clearly seen. This striation is qualitatively consistent with the expected strike point splitting due to magnetic lobe formation. Figure 5 shows the 1-D radial cut of the projected 2-D striations of the formed heat and particle flux lobe structure onto the divertor target. The appearance of multiple peaks and valleys characteristic of lobe structure is seen in both the temperature and D_α profiles after turning on the 3-D field coil. Note that the formation of lobes became visible as quickly as 4-5ms after the 3-D field application, consistent with the estimated ~ 4 ms field penetration time through the vessel and the passive stabilizing plates. Note also that the peak heat and particle flux values are reduced during the 3-D field application.

The observed heat flux striation pattern was compared with the magnetic footprint from a vacuum field line following code, calculated for the toroidal angle of the IR camera. Figure 6 shows that the main characteristics of the heat flux profiles do follow the vacuum field line tracing results, both in the number of the observed striations, and in the relative spacing of the peaks. Note however that the radial locations of the peak heat flux of the lobes slightly differ from those indicated by the vacuum field line tracing result. A comparison between the heat flux and D_α profiles is shown in figure 7. Note that the local peaks in both profiles do not exactly

match. The applied $n=3$ magnetic perturbations are expected to produce the same radial lobe structures for both the IR and visible measurements because the diagnostics are spaced 120° apart. However, the contribution of $n=1$ and $n=2$ components from the intrinsic error fields could result in the different locations for the observed peaks. In general, the heat and particle flux profiles could show different local peaks because they are correlated through convective heat transport, while conductive heat transport is thought to dominate the parallel transport in many NSTX discharges.

A closer look at the structure in the heat and particle flux profiles reveals that the radial position of the local maxima increases with increasing distance from the separatrix (see figure 8), stronger than linearly. It is also observed that the width of the striations in both heat and particle flux profiles increases with increasing distance from the separatrix. The striation widths for D_α and heat flux profiles are larger than the values from the vacuum field line tracing. This is consistent with anticipation because the plasma would diffuse inside the lobes, while the vacuum field line tracing does not consider the plasma response. The effect of three different values of coil current, $I_{RWM}=0.5\text{kA}$, 0.75kA , and 1kA , on heat and particle flux profiles is shown in figure 9. Note that the lowest coil current, $I_{RWM}=0.5\text{kA}$, is below the ELM triggering threshold value of $I_{RWM}=0.75\text{kA}$. Profiles for $I_{RWM}=0.75\text{kA}$ and 1kA were taken before the appearance of triggered ELMs. The magnitude of the peaks and valleys in the IR and D_α profiles was observed to increase with increasing coil current. On the other hand, the spacing between the lobes and the lobe widths are unaffected by the change in the coil current. Within the existing data set, there was no observed minimum threshold for formation the striations..

4. Summary and conclusions

In this paper we have shown that applied 3-D field indeed modifies the heat and particle flux profiles in a manner consistent with vacuum field line tracing in NSTX H-mode plasmas. The measurement shows that the heat flux profile is very sensitive to the applied 3-D field perturbation, forming multiple lobes radially separated on the divertor surface. The D_α profile, used as a proxy to the particle flux profile, also shows clear lobe structures, although the amplitude of the particle flux striations is relatively smaller than the striations in the heat flux profiles. The locations of the lobes in the heat and particle flux profiles match approximately. The structure of lobes for the heat flux and D_α profiles was found to be similar, both for the location and spacing of the lobes. No 3-D field amplitude threshold was observed for lobe formation.

The experimental data also shows that the induced magnetic lobes (or split strike points) broaden both the heat and particle flux profiles and reduce the peak values. For example, about a factor of 2 broadening of the near SOL surface temperature width was observed, compared with

no 3-D field application case. This technique has the prospect for peak heat and particle flux mitigation, particularly in conjunction with fields that are slowly rotated to spread out the peak heat flux locations over time. In coming experiments, we are planning to investigate the effect of various parameter variations such as collisionality, n-number of the applied field, safety factor q_{95} , and heating power, etc, on the lobe structure and its impact on the heat and particle profiles at the divertor plates.

Acknowledgements

The authors are grateful to Dr. J.-K. Park for helpful discussions. This work was funded by the US Department of Energy, contract numbers DE-AC05-000R22725, DE-AC52-07NA27344, and DE-AC02-09CH11466. D.J. Battaglia is supported by the U.S. Department of Energy Fusion Energy Postdoctoral Research Program, administered by the Oak Ridge Institute for Science and Education under contract number DE-AC05-06OR23100.

References

- [1] M. J. Shaffer, J. E. Menard, M. P. Aldan, J. M. Bialek, T. E. Evans and R. A. Moyer, *Nucl. Fusion* **48** (2008), 024004
- [2] J. L. Luxton, *Nucl. Fusion* **42** (2002), 614-33
- [3] K. H. Burrell, T. E. Evans, E. J. Doyle, *et al*, *Plasma Phys. Control. Fusion* **47** (2005) B37-B52
- [4] T. E. Evans, R. A. Moyer, K. H. Burrell, *et al*, *Nature Phys.* **2** (2006) 419-23
- [5] R. A. Moyer, T. E. Evans, T. H. Osborne, *et al*, *Phys. Plasmas* **12** (2005) 056119-11
- [6] T. E. Evans, M. E. Fenstermacher, R. A. Moyer, *et al*, *Nucl. Fusion* **48** (2008) 024002
- [7] M. Ono, S. M. Kaye, Y.-K. M. Peng, *et al*, *Nucl. Fusion* **40** (2000) 557
- [8] R. Maingi, T. H. Osborne, B. P. LeBlanc, *et al*, *Phys. Rev. Lett.* **103** (2009) 075001
- [9] J. M. Canik, R. Maingi, T. Evans, *et al*, IAEA Fusion Energy Conference, Geneva, Switzerland, 2008, EX-D/PD/P1-5
- [10] J. M. Canik, *et al*, "On demand triggering of edge localized instabilities using external non-axisymmetric magnetic perturbations in toroidal plasmas", submitted to *Phys. Rev. Letts.*
- [11] J.M. Canic, *et al*, "ELM destabilization by externally applied non-axisymmetric magnetic perturbations in NSTX", submitted to *Nucl. Fusion*
- [12] P. B. Snyder, H. R. Wilson, T. H. Osborne and A. W. Leonard, *Plasma Phys. Control. Fusion* **46** (2004) A131
- [13] T. E. Evans, R. K. W. Roeder, J. A. Carter, B. I. Rapoport, M. E. Fenstermacher and C. J. Lasnier, *J. Phys : Conf. Ser.* **7** (2005) 174-90
- [14] M. W. Jakubowski, T. E. Evans, M. E. Fenstermacher, *et al*, *Nucl. Fusion* **49** (2009) 095013
- [15] J-W. Ahn, R. Maingi, D. Mastrovito, and A. L. Roquemore, submitted to *Rev. Sci. Instrum.*
- [16] R. Maingi, *M. G. Bell, R. E. Bell, et al*, *Nucl. Fusion* **43** (2003), 969

- [17] S. A. Sabbagh, R. E. Bell, J. E. Menard, *et al*, *Phys. Rev. Lett.* **97** (2006) 045004
- [18] J. E. Menard, M. G. Bell, R. E. Bell, *et el*, *Nucl. Fusion* **47** (2007) S645
- [19] D. Mastrovito, R. Maingi, H. W. Kugel, and A. L. Roquemore, *Rev. Sci. Instrum.* **74** (2003) 5090
- [20] V. A. Soukhanovskii, A. L. Roquemore, C. H. Skinner, *et al*, *Rev. Sci. Instrum.* **74** (2003) 2094
- [21] H. W. Kugel, M. G. Bell, J-W. Ahn, *et al*, *Phys. Plasmas* **15** (2008) 056118

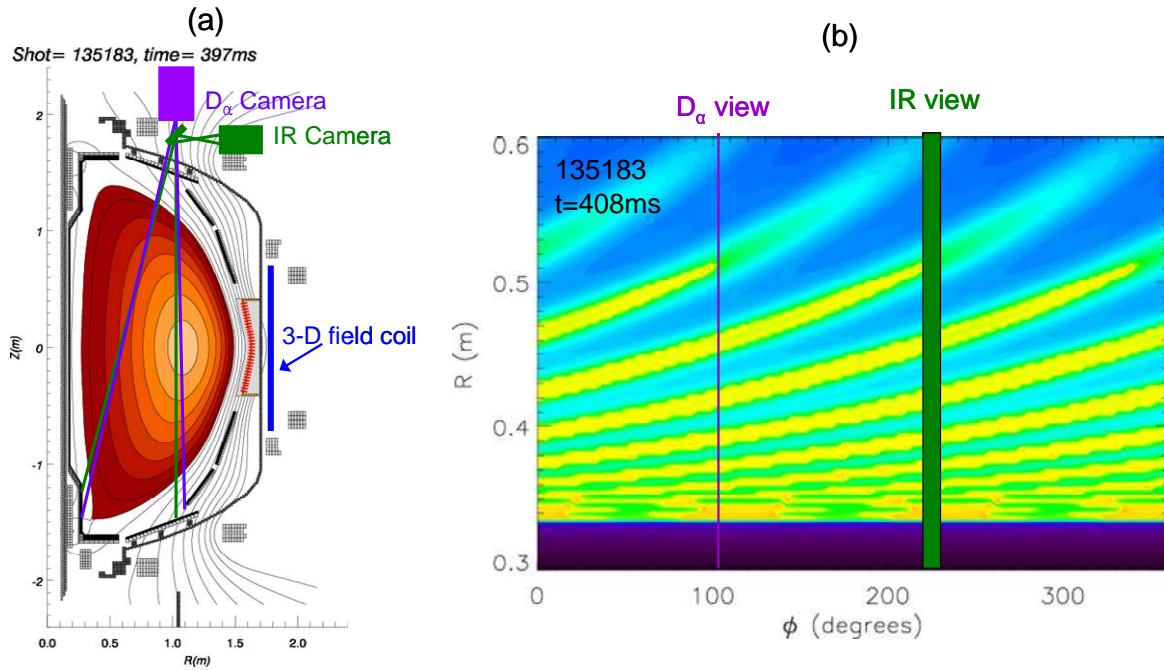


Figure 1. Schematic view of the poloidal cross section of NSTX (a) with magnetic equilibrium reconstruction, field of view of the IR and D_α cameras, and the location of external 3-D field coil overlaid. Figure (b) shows the contour plot of calculated connection lengths showing the formation of lobe structure as a function of toroidal angle (ϕ) and radius. The spatial coverage of D_α and IR cameras is also shown.

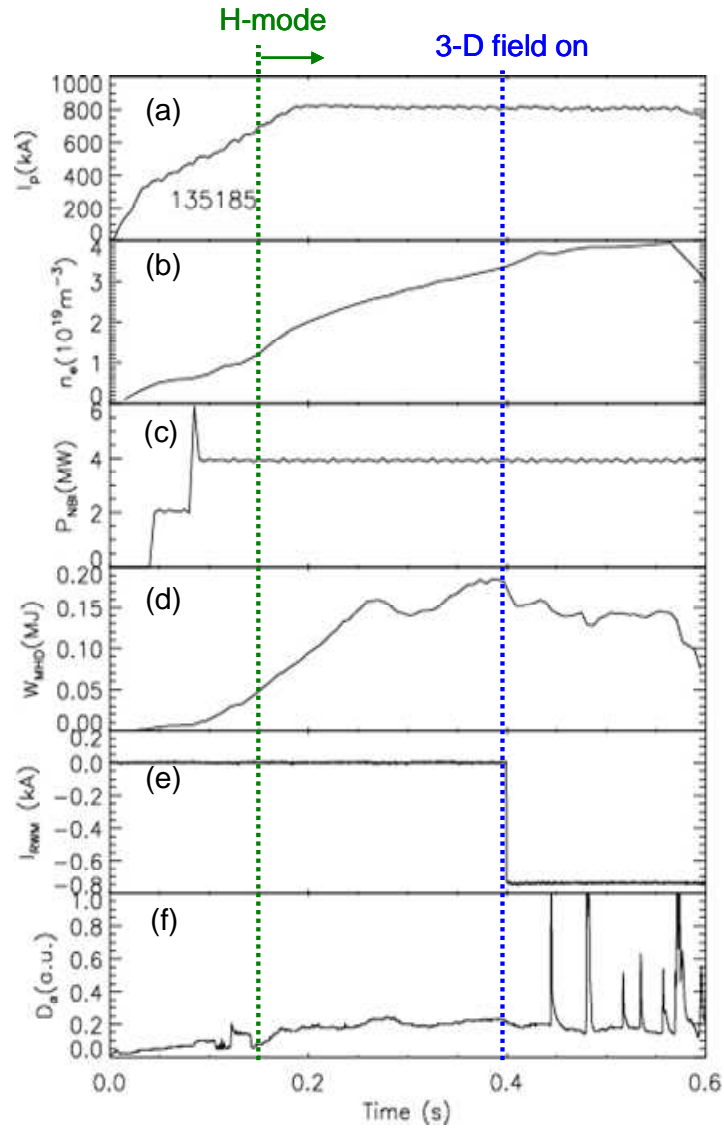


Figure 2. Time evolution of various discharge parameters for a 3-D field applied shot 135185: (a) plasma current, (b) line averaged density, (c) injected NBI power, (d) total stored energy, (e) current in the external 3-D coil, (f) D_α signal for lower divertor. Note that the 3-D field coil was switched on at 400ms

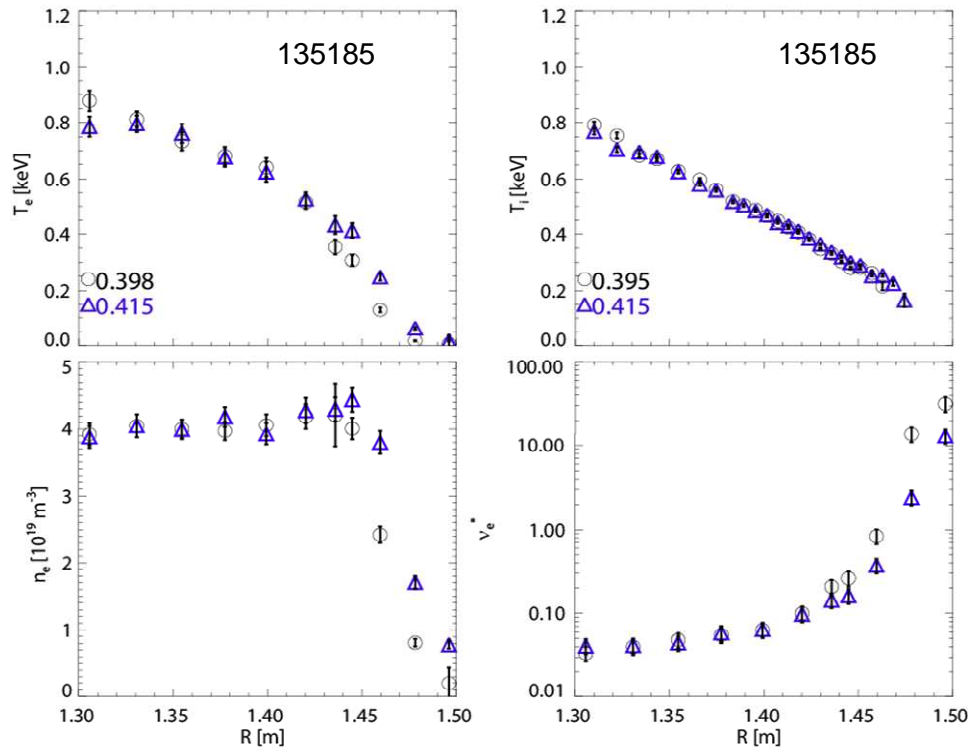


Figure 3. Plasma profiles before ($t=398\text{ms}$) and after ($t=415\text{ms}$) the application of $n=3$ perturbation fields at $t=400\text{ms}$. Note the change in the edge electron profiles after the application.

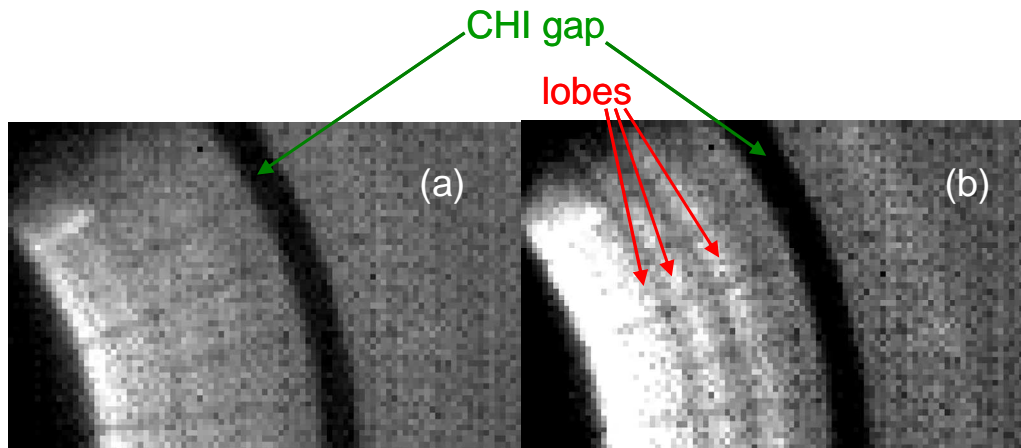


Figure 4. IR images taken 20ms before (a) and after (b) turning on the 3-D field coils at 400ms for shot 135183. Clear formation of lobe structure is seen after the 3-D field application. The “CHI gap” is a gap between inner and outer divertor tiles to enable Coaxial Helicity Injection (CHI) experiment.

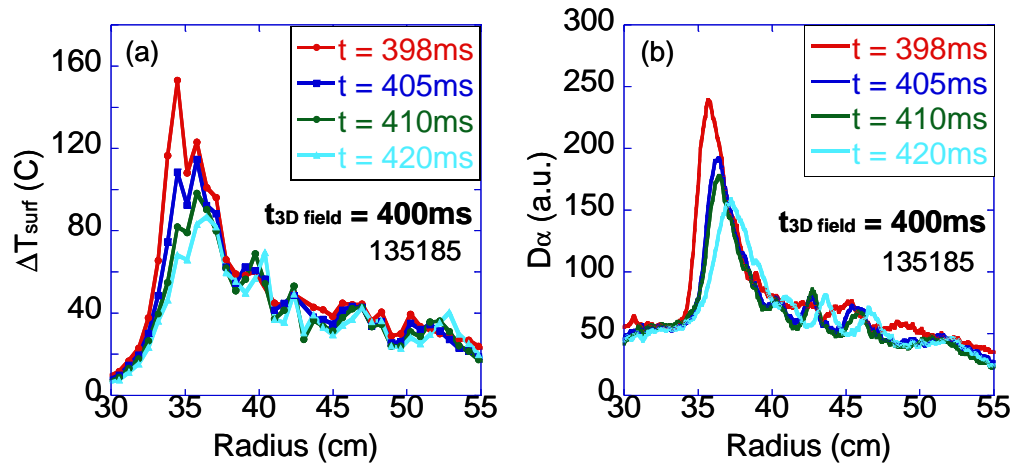


Figure 5. Divertor surface temperature (a) and D_α (b) profiles before and after the 3-D field application at $t=400\text{ms}$. Note the reduced peak values and broadened profiles after the 3-D field application.

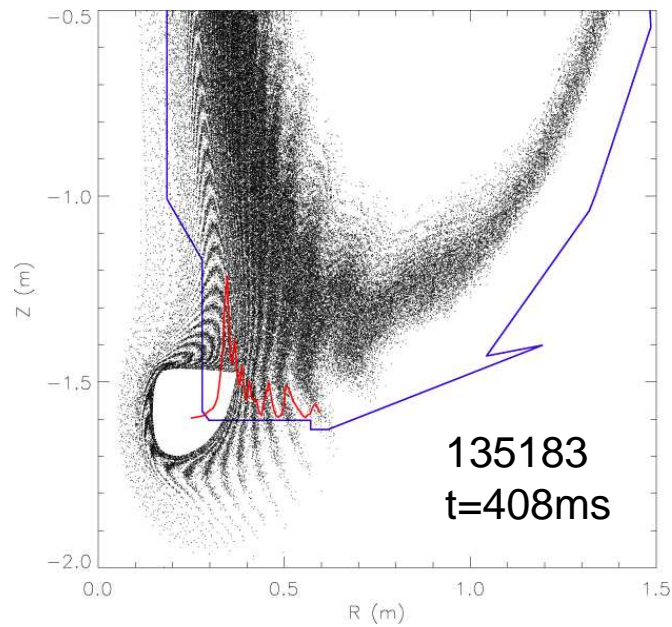


Figure 6. Magnetic footprints on the divertor target, calculated by a vacuum field line tracing code for the toroidal location of the IR camera at $\varphi=225^\circ$, with the measured heat flux profile overlaid (red)

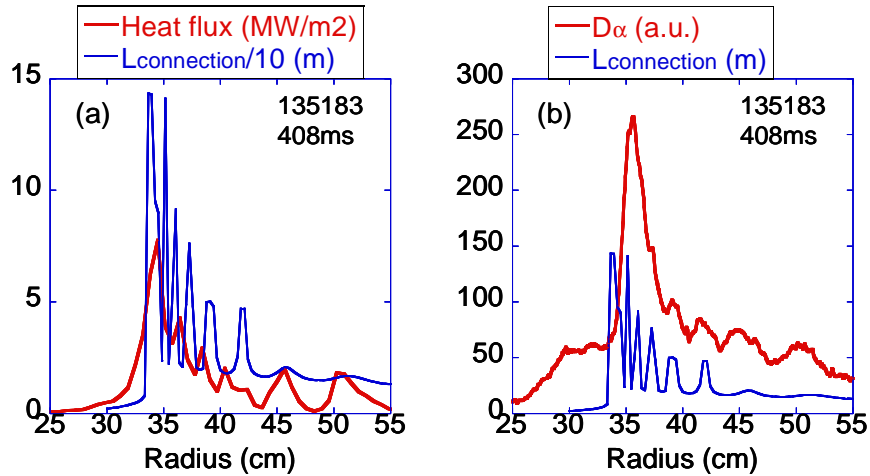


Figure 7. Comparison of heat flux (a) and D_α (b) profiles with calculated connection lengths at the divertor target from the vacuum field line tracing, during the 3-D field application. Note that lobe positions in heat flux and D_α profiles agree only approximately.

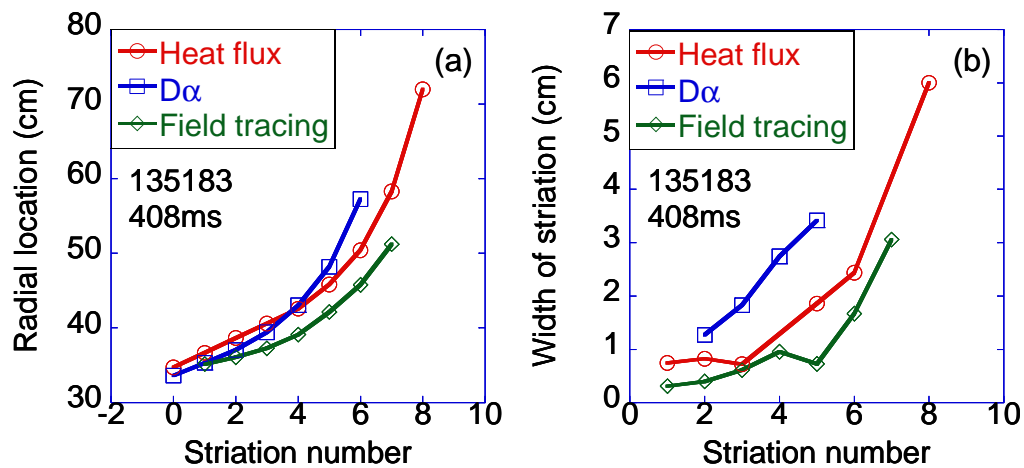


Figure 8. Radial position (a) and the width (b) of lobes vs lobe number during the 3-D field application. Both the radial position and the lobe width increase with increasing lobe number. Here, the width of a lobe was defined as the Full Width Half Maximum (FWHM) of the peak for the corresponding striation in each profile. Data for “field tracing” is from the connection length profile from the vacuum field line tracing, shown in figure 7.

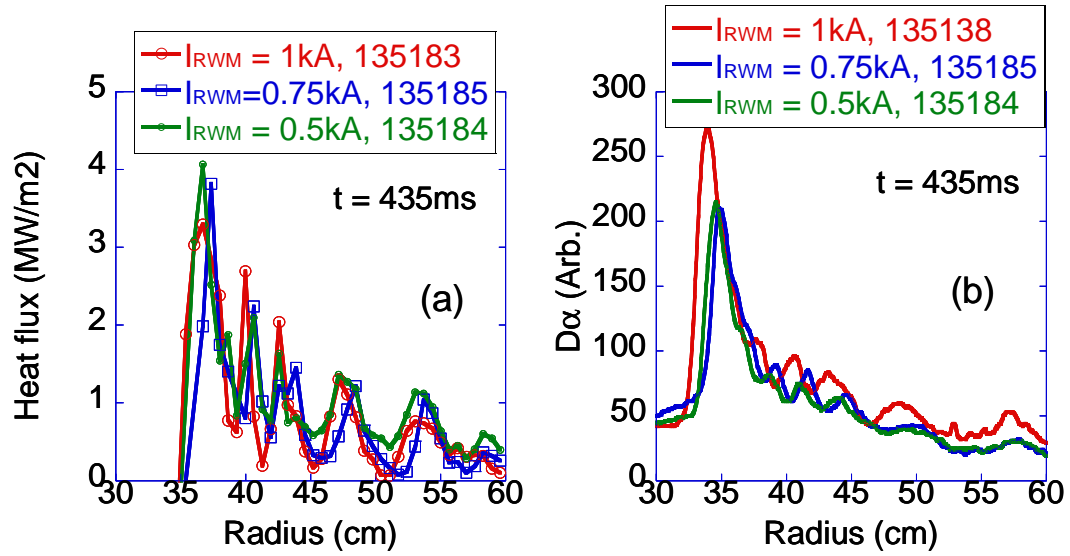


Figure 9. Heat flux (a) and D_α (b) profiles for three different 3-D field coil currents, *i.e.* $I_{RWM}=1\text{kA}$, 0.75kA , and 0.5kA . All three discharges are nominally identical except for the coil currents, for which measurements were carried out at the same time slice ($t=435\text{ms}$) after switching on the coils at $t=400\text{ms}$.